Hyperbolicity, Mach lines and super-shear mode III steady state fracture in magneto-flexoelectric materials: I. Methodology

A.E. Giannakopoulos[1], Ch. Knisovitis[1], A. Charalambopoulos[2], Th. Zisis[1], Ares J. Rosakis[3].

[1] Department of Mechanics, School of Applied Mathematical and Physical Sciences, National Technical University of Athens, Athens, Greece

[2] Department of Mathematics, School of Applied Mathematical and Physical Sciences, National Technical University of Athens, Athens, Greece

[3] Graduate Aerospace Laboratories, California Institute of Technology, Pasadena, CA, USA.

Corresponding author
A. E. Giannakopoulos
Email: agiannak@uth.gr

1. Abstract

This work examines the sub-shear and super-shear steady state growth of mode III fractures in flexoelectric materials, non the less, exhibiting Mach type shock wave patterns that resemble reported lattice dynamics results and three-dimensional calculations and experiments. Our mathematical models provide weak discontinuous solutions of the steady state dynamic equations. In flexoelectric solids, super-shear rupture is possible with Mach lines appearing at sub-shear as well as super-shear crack rupture velocities. This is contrary to classical singular elastodynamics, where the notions of super-shear growth and hyperbolicity coincide. The results show that the deformation near the crack-tip agrees with studies based on lattice dynamics. In the first part of this work, a novel finite element approach has been developed where the problem is decomposed in two prestressed plates which are interconnected, resulting into the predicted radiation patterns and Mach lines. The polarization field is obtained from the calculated displacement field and is used in turn to calculate the magnetic and the electric fields. The analysis offers an analogy to the co-seismic magnetic fields encountered during mode III dominated earthquake rupture events.

Keywords: Magneto-flexoelectricity, mode III crack, hyperbolic, steady state, co-seismic magnetic fields.

2. Introduction

Flexoelectricity describes the coupling between non-uniform strain fields and electric polarization fields in all dielectric materials [1–6]. This universal effect increases with decreasing sampling size and carries great impact on materials and devices. Recent theoretical work on flexoelectrics, including dynamic effects, can be found for example in [7–10]. Mode III fracture is important in several types of failure. For example, mode III delamination growth can occur in a variety of situations encountered in laminated composites. Tvergaard and Hutchinson [11] highlighted the major influence that mode III fracture processes play in thin film delamination problems. Within the context of singular classical elastodynamics, a mode III crack cannot propagate super-sonically in homogeneous solids [12,13]. Yu and Yang [12] investigated the transonic debonding of bimaterial interfaces under anti-plane shear conditions. They found that the debonding speed cannot exceed the higher shear wave speed provided that the energy which flows through the interface is bounded. Forced growth at forbidden velocities may however become possible under crack-tip wedging conditions [14] On the same problem, Huang et al. [15] proved that for propagating mode III interface cracks, a line of stress singularity (Mach line) emitted from the propagating crack-tip is possible only in the material with the smaller shear wave speed [16].

The physical attainability of Mode II super-shear rupture growth was theorized by [14,17–19] in a series of theoretical and numerical works. However, such a phenomenon was never observed in nature up to that time. The first experimental proof of the existence of super-shear rupture was obtained by Rosakis and his co-workers under both conditions of impact (in coherent interfaces) [20] and static far-field loading (in frictional interfaces) [21]. The early work on this subject, including the observation of the mechanism of rupture transition from sub-Rayleigh to super-shear rupture speeds are summarized in two review papers, [22,23], and discussed in the context of classical elastodynamics. Indeed, from the theoretical point of view, transition to super-shear from sub-Rayleigh mode II rupture can be facilitated by assuming the existence of cohesive zones [24]. Moreover, Rosakis [25] showed that when strain gradient effects are included in the Pierls potential, a kinetic relation for the uniformly moving dislocation can predict intersonic and even super-sonic speeds at high enough Peach-Koehler stresses. This observation has provided an early hint of the effect of strain gradients in allowing transitions to both super-shear and even super-sonic rupture speeds and is a motivation for the present study. Super-shear transition may also be found triggered by heterogeneous interfaces (e.g. cohesive stress drop or decrease in fracture energy), see for example [26,27]. Finally, in a three-dimensional rupture setting, local mode III super-shear rupture has been theoretically and experimentally found to follow a predominately mode II super-shear rupture of a plate with finite thickness [28]. For early pioneering work on 3-D self-similar rupture of penny-shaped cracks subjected to shear loading see [29].

In the nano scale, local stiffening of the material due to finite deformation, in a class of lattice models was shown to produce super-shear crack propagation in mode II [30] and super-shear rupture growth in mode II. Atomistic calculations by [13] in mode II and [31] in mode III have predicted super-shear and even super-sonic transitions. Such transitions have also been predicted for mode III ruptures by [32] in the context of large strain elasticity and stiffening potentials.

Although in all cases the authors attribute this phenomenon to the presence of stiffening due to large strains and stiffening at the rupture tip, the presence of locally dominant lattice length scales; pointing to the possible importance of strain gradient effects should also be noted. Moreover, Koizumi et al. [33] also showed that super-shear mode III crack motion is possible for harmonic lattices. They were first to claim that due to the dispersion in a linear lattice, a crack moving at any speed is by definition faster than wave speeds in the part of the dispersion curve in the short wavelength limit. This provides further evidence of the importance of local length scale and strain gradients. The discreteness of their lattice model removes the singular nature of the wave speeds in the long wavelength limit. Koizumi et al. [33] also calculated the radiation patterns of lattice wave emission from moving mode III cracks (mode III super-shear crack growth can be predicted for a stiffening hyperelastic material behavior, with sufficient prestressing [32]). Consistent with the above discussion, Guozden, et al. [34] revisited the super-shear mode III cracking in lattice models and concluded that material stiffening or dissipation are not prerequisites for super-sonic mode III cracking, as long as near tip instabilities are suppressed. They also showed that the crack speed is a function of the strain at the vicinity of the crack-tip.

Sporadic evidence of super-shear rupture bursts has been reported relation to the Imperial Valley Earthquake [35]. Super-shear rupture velocities have also been conclusively documented to occur in large earthquakes such as the 1999 Ismit, the 2002 Denali and the Kunlunshan Earthquakes [36–39]. Such activity has been related to electrokinetic effects [40], which have been shown by Giannakopoulos and Rosakis [41] to be analogous to the magneto-flexoelectric phenomena. However, following the experimental discovery of super-shear rupture velocities in the laboratory [20,21], such large earthquake events may have the ability to trigger measurable electric [42] and magnetic potential change [43,44] and are another motivation for this study. Although such co-seismic emission has long been suspected to occur during large earthquakes [45,46], so far there has been no connection theorized between their occurrence and the presence of super-shear rupture growth prior to the recent work by [41].

The hyperbolic regime of mode III steady state rupture growth in flexoelectrics has first been examined in [47]. The problem decouples to mechanical and to electrical field equations which can be solved in sequence, starting from the autonomous solution of the displacement field and subsequently deriving the associated electrical field. Finally, the steady state electrical field (polarization condition) also produces a steady state electromagnetic field that accompanies the displacement and the polarization field as generally shown by [41]. This offers a possible quantitative explanation of the observed electromagnetic radiation that has been recorded to accompany rock fracture [46,48–50], fracture of ice [51–53] in addition to the electromagnetic activity (via the magneto-flexoelectric - electrokinetic analogy) related to earthquakes discussed above.

Motivated by the laboratory, field observations and modelling analysis discussed earlier, in the first part of this work, we analyze the hyperbolic mode III steady state rupture regime in flexoelectric materials and develop a new finite element methodology to solve the hyperbolic governing equations that control the out-of-plane displacements and ensuing electromagnetic fields. We focus on the development of Mach lines and highlight the differences with the predictions of classic elastodynamics. Then-on, we also capture and analyze the polarization

and the magnetic fields that follow the displacement problem. In the second part of this paper, we focus on the asymptotic analysis in the vicinity of the crack-tip.

3. The general formulation

Under anti-plane formulation the flexoelectric problem has two primary variables: the out-of-plane displacement $u_3(x_1, x_2, t)$ [m] and the out-of-plane polarizations $P_3(x_1, x_2, t)$ [Cm^{-2}], where x_1, x_2 are the plane coordinates and t is the time. The energy density of a flexoelectric material can be written as (where $(\cdot)_{,i} = \partial(\cdot)/\partial x_i$):

$$U = \frac{1}{2}\left\{ aP_3^2 + \left(b_{44} + b_{77}\right)\left(P_{3,1}^2 + P_{3,2}^2\right) + 2e_{44}\left[\left(\varepsilon_{13} + \varepsilon_{31}\right)P_{3,1} + \left(\varepsilon_{23} + \varepsilon_{32}\right)P_{3,2}\right] \right.$$
$$\left. + 2f_{12}\left[\left(\varepsilon_{13,1} + \varepsilon_{31,1}\right)P_3 + \left(\varepsilon_{23,2} + \varepsilon_{32,2}\right)P_3\right] + 2\mu\left(\varepsilon_{13}^2 + \varepsilon_{23}^2\right)\right\} \tag{3.1}$$

For the general formulation see [54–56]. Giannakopoulos and Zisis [47,57,58], have shown that in the absence of body forces and initial electric field, one can write the following two uncoupled p.d.e.'s with respect to the two primary variables of the problem ($\ddot{u}_3 = \partial^2 u_3/\partial t^2$).

1. The displacement equation (wave equation):

$$\mu\nabla^2 u_3 - \mu\frac{\ell^2}{2}\nabla^4 u_3 = \rho\ddot{u}_3 - \frac{\rho H^2}{12}\nabla^2\ddot{u}_3 \tag{3.2}$$

2. The polarization equation (follower equation) of the anti-plane flexoelectric problem is:

$$P_3 - \frac{\ell^2}{2}\nabla^2 P_3 = \frac{\rho\left(e_{44} - f_{12}\right)}{\mu a}\ddot{u}_3 \tag{3.3}$$

In eqs (3.2) and (3.3) we find a "microstructural length" $\ell/\sqrt{2}$ and a "micro-inertial length" $H/\sqrt{12}$ related to the corresponding flexoelectric parameters:

$$\frac{\ell^2}{2} = \frac{b_{44} + b_{77}}{a} - \frac{\left(e_{44} - f_{12}\right)^2}{\mu a} \geq 0 \tag{3.4.a}$$

$$\frac{H^2}{12} = \frac{b_{44} + b_{77}}{a} \geq \frac{\ell^2}{2} \tag{3.4.b}$$

The material constants are the atomistic radius a_0[m], the density ρ[kg m^{-3}], the shear modulus μ [N m^{-2}], the flexoelectric constant f_{12} [N m C^{-1}], the reciprocal dielectric constant a [N m^2 C^{-2}], the inverse flexoelectric constant e_{44} [N m C^{-1}], the gradient polarization constant $(b_{44}+b_{77})$ [N m^4 C^{-2}] and $P_{\max}$ [C/ m^2] is the polarization strength. Typical values of the constants of some flexoelectric materials are shown in Table 1 [57]. Note that the material parameters must obey the inequalities suggested by eqs. (3.4.a) and (3.4.b), in order for the energy density to be positive definite and hence provide uniqueness conditions. Otherwise, the constitutive laws must include other stabilizing terms, e.g. strain gradient effects [59].

Table 1.   The characteristic constants of three flexoelectric materials [57].

Parameter	Dimension	Material		
		SrTiO$_3$	KTaO$_3$	KCℓ
a_0	nm	0.391	0.399	0.314
ρ	kg/m^3	5174	6970	1980
$c_{44} = \mu$	GPa	122	107	6.8
a	10^8 N m^2/C^2	2.12	0.355	243
$b_{44}+b_{77}$	10^{-9} N m^4/C^2	2.00	0.435	1.20
$e_{44}-f_{12}$	N m/C = V	-10.00	6.00	-2.15
$P_{\max}$	mC/cm^2	42	24	–
c_s	m /s	4856	3910	1853
$H/\sqrt{12}$	nm	3.07	3.50	0.222
$\ell/\sqrt{2}$	nm	2.36	1.66	0.146
$H/(\ell\sqrt{6})$	–	1.30	2.11	1.52

In Figure 1 we show the steady state mode III (anti-plane) crack problem with constant rupture velocity V in an infinite plane (x_1, x_2). The fields u_3 and P_3 are antisymmetric with respect to the $x_2 - axis$. According to Figure 1, the steady state problem can be casted by changing the coordinates to a moving with the crack-tip coordinate system:

$$\xi = x_1 + Vt \tag{3.5.a}$$

$$\eta = x_2 \tag{3.5.b}$$

and thus, (3.2) transforms to:

$$\left(1 - \frac{V^2}{c_s^2}\right)\frac{\partial^2 u_3}{\partial \xi^2} + \frac{\partial^2 u_3}{\partial \eta^2} - \frac{\ell^2}{2}\left(1 - \frac{V^2 H^2}{6\ell^2 c_s^2}\right)\frac{\partial^4 u_3}{\partial \xi^4} - \frac{\ell^2}{2}\left(2 - \frac{V^2 H^2}{6\ell^2 c_s^2}\right)\frac{\partial^4 u_3}{\partial \xi^2 \partial \eta^2} - \frac{\ell^2}{2}\frac{\partial^4 u_3}{\partial \eta^4} = 0 \quad (3.6)$$

5

This differential equation must be solved for $u_3(\xi,\eta)$ with the proper boundary conditions (B.C.). The traction type boundary conditions are;

$$\left[-\frac{\ell^2}{2}\frac{\partial^3 u_3}{\partial \eta^3} - \ell^2 \frac{\partial^3 u_3}{\partial \eta \partial \xi^2} + \frac{H^2 V^2}{12 c_s^2}\frac{\partial^3 u_3}{\partial \eta \partial \xi^2} + \frac{\partial u_3}{\partial \eta} \right] = \frac{t_3(\xi)}{\mu} \tag{3.7}$$

$$\frac{\ell^2}{2}\frac{\partial^2 u_3}{\partial \eta^2} = \frac{r_3(\xi)}{\mu} \tag{3.8}$$

where $t_3(\xi)[N/m^2]$ and $r_3(\xi)[N/m]$ are described along the crack face and according to [56]; $r_3(\xi) = f_{44} P_3(\xi)$. The kinematic conditions conjugate to (3.7) and (3.8) are u_3 and $\partial u_3 / \partial \eta$ respectively. Interestingly, eqs. (3.6) - (3.8) are similar to those obtained in couple stress elasticity under anti-plane steady state conditions [60] and in dipolar gradient elasticity [61].

The steady state differential equation of the polarization in the flexoelectric anti-plane problem can be obtained from (3.3):

$$P_3 - \frac{\ell^2}{2}\left(\frac{\partial^2 P_3}{\partial \xi^2} + \frac{\partial^2 P_3}{\partial \eta^2} \right) = V^2 \frac{\rho(e_{44} - f_{12})}{a\mu}\frac{\partial^2 u_3}{\partial \xi^2} \tag{3.9}$$

Depending on the magnitude of the microstructural length ratio $H/(\ell\sqrt{6})$, the character of eq. (3.6) may change from elliptic to hyperbolic in respect to the values of the ratios $(\rho V^2 H^2)/(6\mu\ell^2)$ and $H/(\ell\sqrt{6})$ (see Figure 2). The present work focuses on the hyperbolic conditions:

$$\frac{\rho V^2 H^2}{6\mu\ell^2} > 1, \quad \frac{H}{\ell\sqrt{6}} \geq 1. \tag{3.10}$$

The second inequality of (3.10) comes from (3.4). Depending on the magnitude of the rupture velocity V, we may have sub-shear cracking, if

$$V < \sqrt{\frac{\mu}{\rho}} = c_s \tag{3.11}$$

or super-shear if

$$V > c_s \tag{3.12}$$

We must emphasize that the hyperbolic conditions (3.10) do not imply necessarily super-shear rupture, as is the case for classical elastodynamics. Thus, Mach lines are expected even for sub-shear conditions, as found in lattice dynamics [33,62]. Note, that the condition $\rho V^2 H^2 (6\mu\ell^2)^{-1} = 1$ together with $V/c_s = 1$ constitute boundaries of a sub-Rayleigh region. In flexoelectricity, mode III supports the development of Rayleigh anti-plane surface waves along the crack faces [47,57,58].

4. The out-of-plane displacement

Under hyperbolic conditions eq. (3.6) can be solved with the method of the characteristic lines. Accordingly, the characteristic coordinates can be written as follows;

$$\bar{\eta} = \frac{\xi}{\ell} \pm \frac{\eta}{\ell}\,\bar{a} \tag{4.1.a}$$

where:

$$\bar{a} = \sqrt{\frac{H^2 V^2}{6\ell^2 c_s^2} - 1} \tag{4.1.b}$$

$$c_s = \sqrt{\frac{\mu}{\rho}}$$
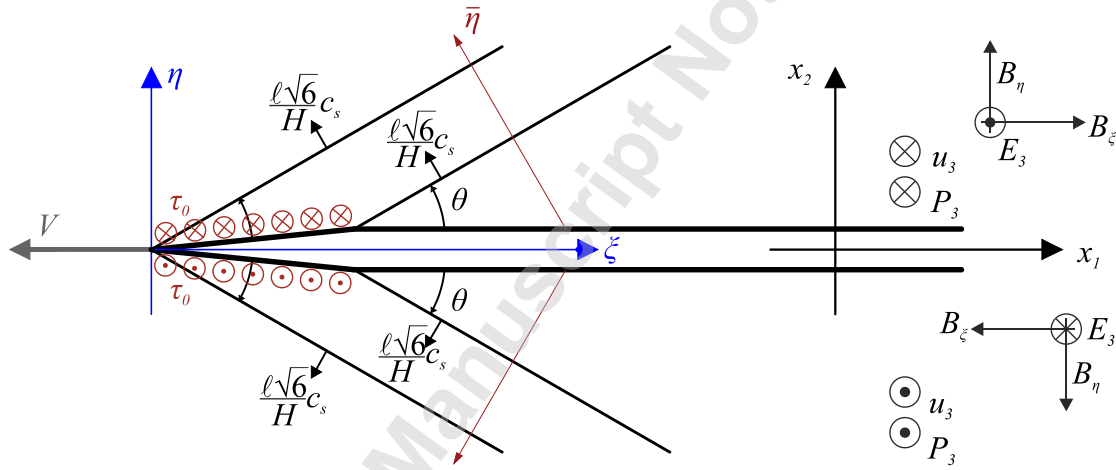
$$\sin\theta = \frac{\ell\sqrt{6}}{H}\frac{c_s}{V}$$

Figure 1.   The coordinate system of a crack-tip moving with the crack-tip constant rupture velocity V, the loading of the moving crack surfaces and the possible Mach lines that emanate from the crack-tip region. u_3 is the out of plane displacement field, $\dot{u}_3 = V\,\partial u_3/\partial\xi$ is the velocity field, P_3 is the polarization field, E_3 is the electric field and (B_ξ, B_η) is the magnetic flux. The traction B.C. at $\eta = 0^+$ and $\xi \geq 0$ are $t_3(\xi) = -\tau_0(\langle\xi\rangle^0 - \langle\xi - L\rangle^0)$ and $r_3(\xi) \approx 0$. See also Appendix B for conditions at $\xi = 0$ and $\xi = L$.
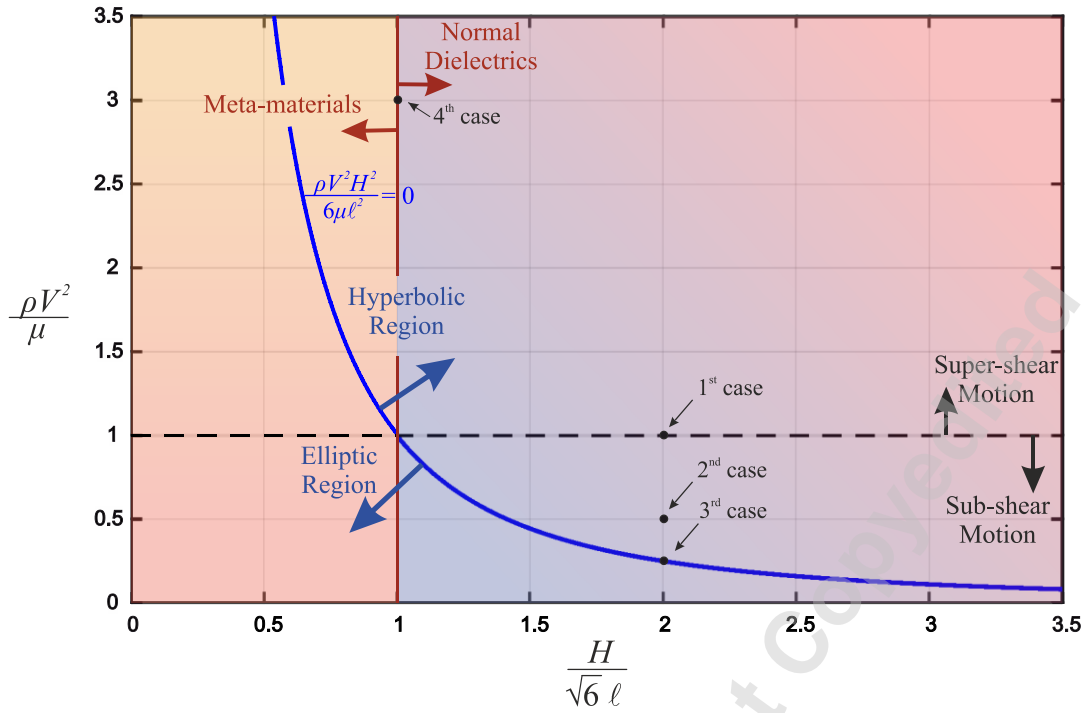
Figure 2. The elliptic and hyperbolic regions that appear in a steady state dynamic anti-plane flexoelectric problem (based on a similar figure from [47,57,58] and [60]. Note that for classic elastodynamics the hyperbolic region is also the super-shear region.

Using eq. (4.1.a), we obtain $\bar{h} = \ln u_3$ and eq. (3.2) leads to:

$$\left[\frac{\partial^2 \bar{h}(\bar{\eta})}{\partial \bar{\eta}^2} + \left(\frac{\partial \bar{h}(\bar{\eta})}{\partial \bar{\eta}} \right)^2 \right] \left(\frac{H^2 V^2}{6\ell^2 c_s^2} - \frac{V^2}{c_s^2} \right) = 0 \qquad (4.2)$$

The general solution of eq. (4.2) can be found in [57]. Note that if $H/\ell\sqrt{6} = 1$ eq (4.2) does not exist and therefore the problem will return to the classic one (absence of hyperbolic region).

In what follows we assume that the faces of the crack ($\eta = 0$) are loaded with a constant shear traction $t_3 = \tau_0$, close to the crack-tip in the region $0 \le \xi \le L$ and $r_3 = 0$ for $\xi > 0$, as shown in Figure 1 [63]. This loading follows the moving crack-tip and can be though of as a load due to an explosion that propagates with velocity V [64]. Another way to apply such loading conditions is through irradiation with a focussed laser which induces expanding plasma inside the expanding crack, as in the case of $KC\ell$ crystals [65,66]. Further more, [67] managed to apply wedge indentation loading on ice and observed crack tip velocities higher than the shear wave of ice. Supersonic cleavage of an elastic strip by a thin smooth rigid wedge was found to be also possible [68].

8

If we consider the possibility of strain discontinuities, a solution of the hyperbolic differential equation (4.2) is [69];

$$u_3(\bar{\eta}) = -\frac{u_L}{L/\ell}\langle\bar{\eta}\rangle + \frac{u_L}{L/\ell}\langle\bar{\eta} - L/\ell\rangle \qquad (4.3.a)$$

where $\langle...\rangle$ is the Macauley brackets of first order and:

$$u_L = \frac{\tau_0 L}{\bar{a}\mu} \qquad (4.3.b)$$

This solution implies a critical strain $u_L / L = \tau_0 / (\mu\bar{a}) = \gamma_c$. Note, that [34] suggested a value of theoretical strain $\gamma_c = 0.24$. The schematic of this approximation is shown in Figure 3. Planar wave fronts emanate from leading and trailing edges of the loading lines, as indicated in mode II dynamic rupture pulses (see for example [70]). At the crack tip $(\xi = 0)$ and at the end of the loading region $(\xi = L)$, Mach lines are essential shock waves that will allow the crack-tip motion. The corresponding jump conditions are discussed in the Appendix A. The solution satisfies the energy conservation implying that the strain energy in the unfractured material is converted completely into kinetic energy as the crack propagates, as found for the classic elastodynamics by [71]. This means that the energy release rate is zero for this particular type of solution and thus, the fast crack propagation is dominated by the conversion of strain energy into kinetic energy, with the surface energy assumed to be rather small due to some prior weakness in the rupture direction. Additional consideration regarding the crack tip asymptotes when the strains are continuous will be given in the second part of this paper [72].
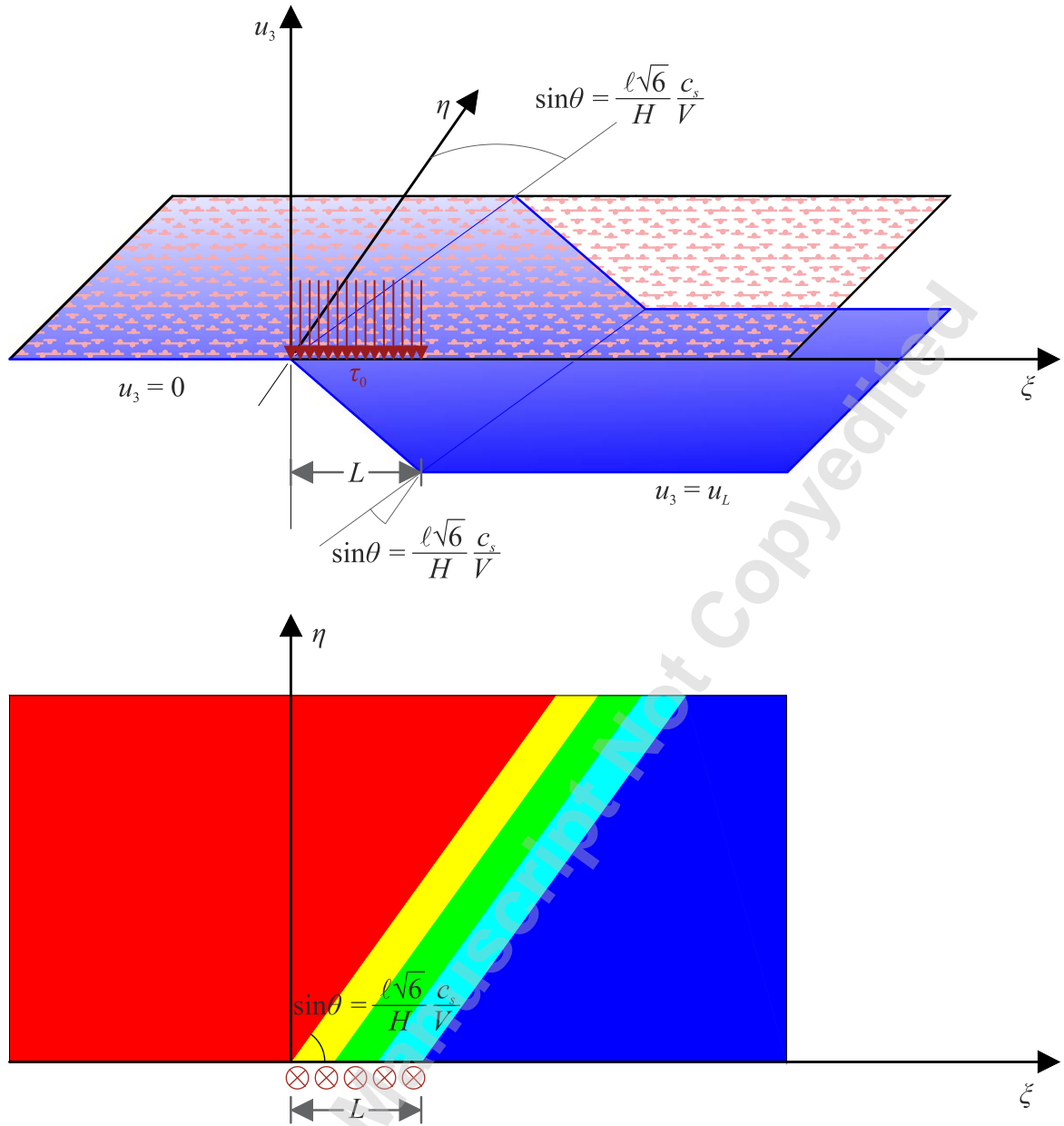
Figure 3. The out of plane deformation in the hyperbolic case, as suggested by the approximation (4.3.a).

The general form of the hyperbolic equation with respect to u_3 is:

$$\left[A_1 \frac{\partial^4}{\partial \xi^4} + 2 A_2 \frac{\partial^4}{\partial \xi^2 \partial \eta^2} + A_3 \frac{\partial^4}{\partial \eta^4} - \left(B_1 \frac{\partial^2}{\partial \xi^2} + B_2 \frac{\partial^2}{\partial \eta^2} \right) \right] u_3 (\xi, \eta) = p(\xi, \eta) \qquad \text{(4.4.a)}$$

$$A_1 < 0, \quad A_1 > A_2, \quad A_3 > 0, \quad B_1 > 0 \qquad \text{(4.4.b)}$$

If $A_1 > 0$, then eq. (4.4.a) is elliptic and is equivalent to the equation of an orthotropic prestressed plate with zero Poisson's ratio [73]. Between eq (4.4.a) and the orthotropic

10

prestressed plate with zero Poisson's ration [74] it has been shown by [58] that the following analogies hold (see Table 2). In Table 2, h [m] is the plate's thickness, (N_ξ, N_η) [Nm^{-1}] are the prestress line forces, (E_ξ, E_η) [Nm^{-2}] are the elastic moduli and Q_0 [Nm^{-1}] is the line shear force

Table 2.   The analogies between the anti-plane couple elasticity problem and the prestressed orthotropic plate as introduced by [47,58].

	Anti-plane problem (Elliptic Case)	Plate Problem
$A_1 \equiv A_1^{og}$	$\dfrac{\ell^2}{2}\left(1 - \dfrac{V^2 H^2}{6\ell^2 c_s^2}\right)$	$\dfrac{E_\xi h^3}{12 N_\eta}$
$2A_2 \equiv 2A_2^{og}$	$\dfrac{\ell^2}{2}\left(2 - \dfrac{V^2 H^2}{6\ell^2 c_s^2}\right)$	$\dfrac{G_{\xi\eta} h^3}{3 N_\eta}$
$A_3 \equiv A_3^{og}$	$\dfrac{\ell^2}{2}$	$\dfrac{E_\eta h^3}{12 N_\eta}$
$B_1 \equiv B_1^{og}$	$1 - \dfrac{V^2}{c_s^2}$	$\dfrac{N_\xi}{N_\eta}$
$B_2 \equiv B_2^{og}$	1	1
	μ	$\dfrac{N_\eta}{h}$
	τ_0	$\dfrac{Q_0}{h}$

However, in the present case $A_1 < 0$ and the plate analogue found for the elliptic case must be modified. A decomposition of eq. (4.4.a) suggest that:

$$\left[A_1\left(\frac{\partial^2}{\partial \xi^2} - \lambda_1 \frac{\partial^2}{\partial \eta^2}\right)\left(\frac{\partial^2}{\partial \xi^2} - \lambda_2 \frac{\partial^2}{\partial \eta^2}\right) - \left(B_1 \frac{\partial^2}{\partial \xi^2} + B_2 \frac{\partial^2}{\partial \eta^2}\right)\right] u_3(\xi,\eta) = p(\xi,\eta) \quad (4.5.a)$$

$$\lambda_1 = \frac{-A_2 + \left|\sqrt{A_2^2 - A_1 A_3}\right|}{A_1} < 0 \quad (4.5.b)$$

$$\lambda_2 = \frac{-A_2 - \left|\sqrt{A_2^2 - A_1 A_3}\right|}{A_1} > 0 \quad (4.5.c)$$

Then, the analogue equation method decomposition [75] (see also [76]) can be used to split eq. (4.5.a) into two simultaneously operating partial differential equations according to:

11

$$\left(-A_1\lambda_2\frac{\partial^4}{\partial\xi^2\partial\eta^2} + A_1\lambda_1\lambda_2\frac{\partial^4}{\partial\eta^4} - B_2\frac{\partial^2}{\partial\eta^2} \right) u_3(\xi,\eta) = p(\xi,\eta) + b(\xi,\eta) \qquad (4.6.a)$$

$$\left(-A_1\frac{\partial^4}{\partial\xi^4} + A_1\lambda_1\frac{\partial^4}{\partial\xi^2\partial\eta^2} + B_1\frac{\partial^2}{\partial\xi^2} \right) u_3(\xi,\eta) = b(\xi,\eta) \qquad (4.6.b)$$

Equations (4.6.a), (4.6.b) suggests a two plate analogue, as summarized in Table 3. Both plate equations must be solved simultaneously with the same boundary conditions applied to both equations. Therefore, eqs (4.6.a), (4.6.b) can be modelled by a combination of two coupled plates, as will be shown in following section. Interior estimates regarding the continuity and finiteness of p, b, u_3 and their derivatives can be found in [77].

Table 3.   The decomposition of the hyperbolic differential equation of the anti-plane flexoelectric problem into two parabolic analogue equations.

The original Equation
$$\left[A_1\frac{\partial^4}{\partial\xi^4} + 2A_2\frac{\partial^4}{\partial\xi^2\partial\eta^2} + A_3\frac{\partial^4}{\partial\eta^4} - \left(B_1\frac{\partial^2}{\partial\xi^2} + B_2\frac{\partial^2}{\partial\eta^2} \right) \right] u_3(\xi,\eta) = p(\xi,\eta)$$
The First Analogue Problem
$$\left[\left(A_2 + \left| \sqrt{A_2^2 - A_1A_3} \right| \right)\frac{\partial^4}{\partial\xi^2\partial\eta^2} + A_3\frac{\partial^4}{\partial\eta^4} - B_2\frac{\partial^2}{\partial\eta^2} \right] u_3(\xi,\eta) = p(\xi,\eta) + b(\xi,\eta)$$
The Second Analogue Problem
$$\left[-A_1\frac{\partial^4}{\partial\xi^4} + \left(-A_2 + \left| \sqrt{A_2^2 - A_1A_3} \right| \right)\frac{\partial^4}{\partial\xi^2\partial\eta^2} + B_1\frac{\partial^2}{\partial\xi^2} \right] u_3(\xi,\eta) = b(\xi,\eta)$$

The First Analogue	The Second Analogue
$A_1^{I} = 0$	$A_1^{II} = -A_1^{og}$
$2A_2^{I} = A_2^{og} + \left\| \sqrt{A_2^{og}A_2^{og} - A_1^{og}A_3^{og}} \right\|$	$2A_2^{II} = -A_2^{og} + \left\| \sqrt{A_2^{og}A_2^{og} - A_1^{og}A_3^{og}} \right\|$
$A_3^{I} = A_3^{og}$	$A_3^{II} = 0$
$B_1^{I} = 0$	$B_1^{II} = -B_1^{og}$
$B_2^{I} = B_2^{og}$	$B_2^{II} = 0$

12

Table 4.   The analogue modified according to the decomposition proposed in Figure 4.

Orig. Prob.	Decomposed Problem	Analogue Plate problem	The FEM implementation
The First Analogue (1st plate)			
A_1	$A_1^I = 0$	$\dfrac{E_\xi^I h^3}{12 N_\eta^I}$	$E_\xi^I = 0$
$2A_2$	$2A_2^I = A_2^{og} + \left\lvert \sqrt{A_2^{og} A_2^{og} - A_1^{og} A_3^{og}} \right\rvert$	$\dfrac{G_{\xi\eta}^I h^3}{3 N_\eta^I}$	$G_{\xi\eta}^I = \dfrac{1}{8}\left(\dfrac{12\mu}{h^2}\dfrac{\ell^2}{2}\right)\left[\left(2 - \dfrac{V^2 H^2}{6\ell^2 c_s^2}\right) \right.$ $\left. + \left\lvert\sqrt{\left(2 - \dfrac{V^2 H^2}{6\ell^2 c_s^2}\right)^2 - 4\left(1 - \dfrac{V^2 H^2}{6\ell^2 c_s^2}\right)}\right\rvert\right]$
A_3	$A_3^I = A_3^{og}$	$\dfrac{E_\eta^I h^3}{12 N_\eta^I}$	$E_\eta^I = \dfrac{12\mu}{h^2}\dfrac{\ell^2}{2}$
B_1	$B_1^I = 0$	$\dfrac{N_\xi^I}{N_\eta^I}$	$N_\xi^I = 0$
B_2	$B_2^I = B_2^{og}$	1	$N_\eta^I = \mu\, h$
The Second Analogue (2nd plate)			
A_1	$A_1^{II} = -A_1^{og}$	$\dfrac{E_\xi^{II} h^3}{12 N_\eta^{II}}$	$E_\xi^{II} = -\left(1 - \dfrac{V^2 H^2}{6\ell^2 c_s^2}\right)\left(\dfrac{12\mu}{h^2}\dfrac{\ell^2}{2}\right)$
$2A_2$	$2A_2^{II} = -A_2^{og} + \left\lvert \sqrt{A_2^{og} A_2^{og} - A_1^{og} A_3^{og}} \right\rvert$	$\dfrac{G_{\xi\eta}^{II} h^3}{3 N_\eta^{II}}$	$G_{\xi\eta}^{II} = \dfrac{1}{8}\left(\dfrac{12\mu}{h^2}\dfrac{\ell^2}{2}\right)\left[-\left(2 - \dfrac{V^2 H^2}{6\ell^2 c_s^2}\right) \right.$ $\left. + \left\lvert\sqrt{\left(2 - \dfrac{V^2 H^2}{6\ell^2 c_s^2}\right)^2 - 4\left(1 - \dfrac{V^2 H^2}{6\ell^2 c_s^2}\right)}\right\rvert\right]$
A_3	$A_3^{II} = 0$	$\dfrac{E_\eta^{II} h^3}{12 N_\eta^{II}}$	$E_\eta^{II} = 0$
B_1	$B_1^{II} = -B_1^{og}$	$\dfrac{N_\xi^{II}}{N_\eta^{II}}$	$N_\xi^{II} = -\left(1 - \dfrac{V^2}{c_s^2}\right)\mu\, h$
B_2	$B_2^{II} = 0$	1	$N_\eta^{II} = \mu\, h$

13

5. The finite element method (FEM)

The finite element model described in the previous section is shown schematically in Figure 4 and was implemented in the ABAQUS [78] general purpose FEM code. The model consists of two identical plates whose nodes are connected by stiff vertical struts of height h_b, so that both plates' nodes share the same vertical displacement, corresponding to the anti-plane unknown field $u_3(\xi, \eta)$. The two plates have the same boundary conditions, but different plate properties and different levels of prestresses, as summarized in Table 4. Essentially the two plates have lost their bending stiffness in each direction ξ and η, respectively. The refined finite element mesh used in our calculations consists of 80000 triangular plate elements evenly distributed in order to capture the localized increased displacement gradients suggested by the prior analysis (Figure 5.a). In this way, the modified problem (eq. (4.6.a) and eq. (4.6.b)) is solved with a more stable numerical methodology than the initial problem (eq. (4.5.a)). The loading region L was resolved with about 11 elements. In part II, for the asymptotic analysis, L was resolved with about 100 elements and $\ell / \sqrt{2}$ with 15 elements. For the present analysis, the additional analogies are as follows:

1. The out of plane shear loading (Figure 5)

$$\tau_0 = \frac{2 Q_0}{2h + h_b} \frac{L^2}{\ell^2 / 2} \tag{5.1}$$

2. The microstructural length

$$\frac{\ell^2}{2} = \frac{E_\eta^I \, h^3}{12 \, N_\eta^I} \tag{5.2}$$

3. The shear modulus

$$\mu = \frac{N_\eta^I}{h} \tag{5.3}$$

The results of the FEM calculations for four selected cases in the hyperbolic regime (depicted in Figure 2) are shown in Figure 6. Note the development of Mach cones as suggested by the theory, even for sub-shear rapture velocities.

The asymptotic field near the crack-tip will be presented in the second part of this work.
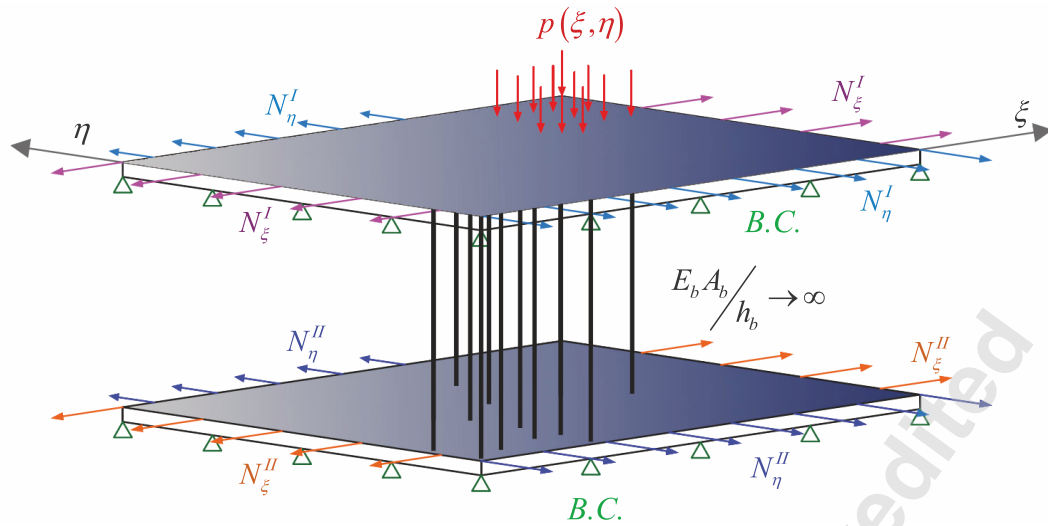
14

Figure 4.   A schematic representation of the two-plate analogue configuration as introduced in ABAQUS.
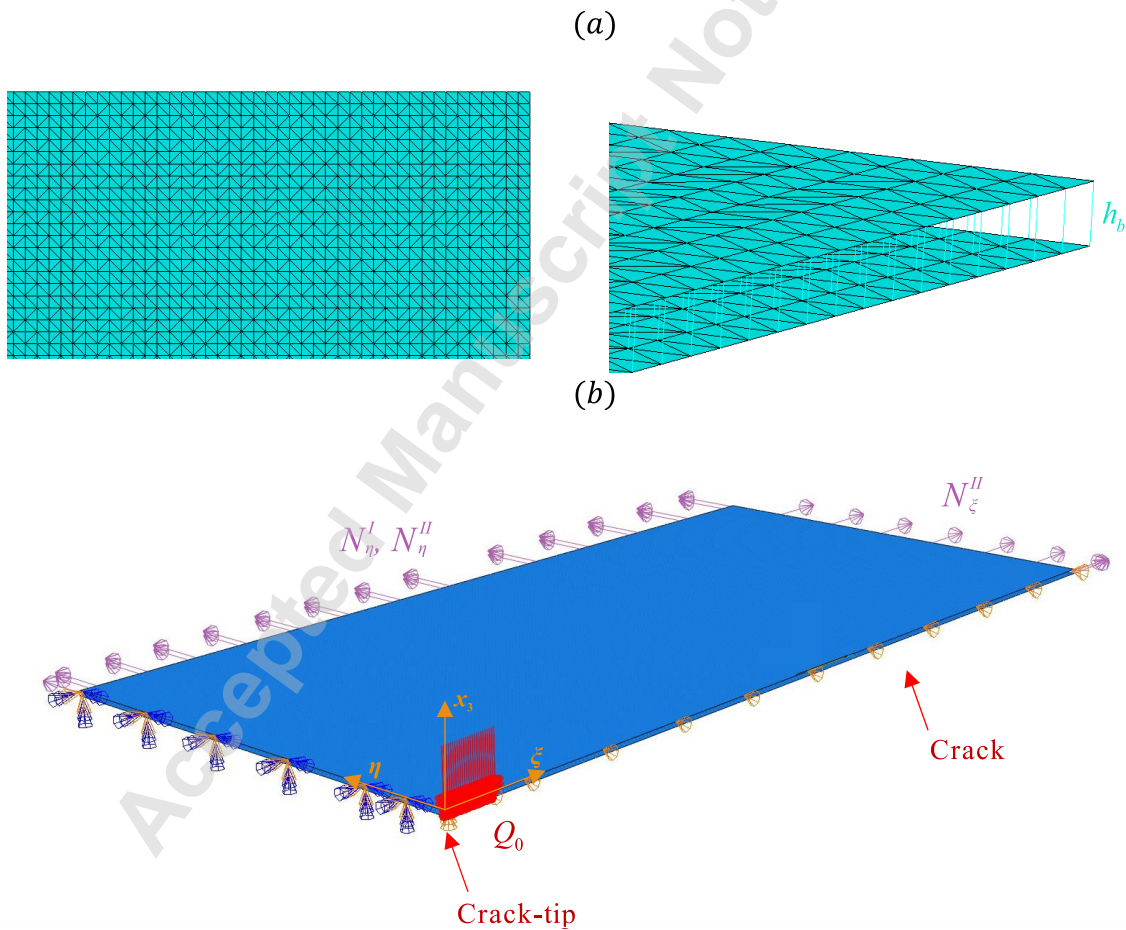

Figure 5.   (a), The discretization of the FEM model. (b), The boundary conditions. The final model contains 40000 three-noded shell elements for each plate and 20301 beam elements to connect the two plates.
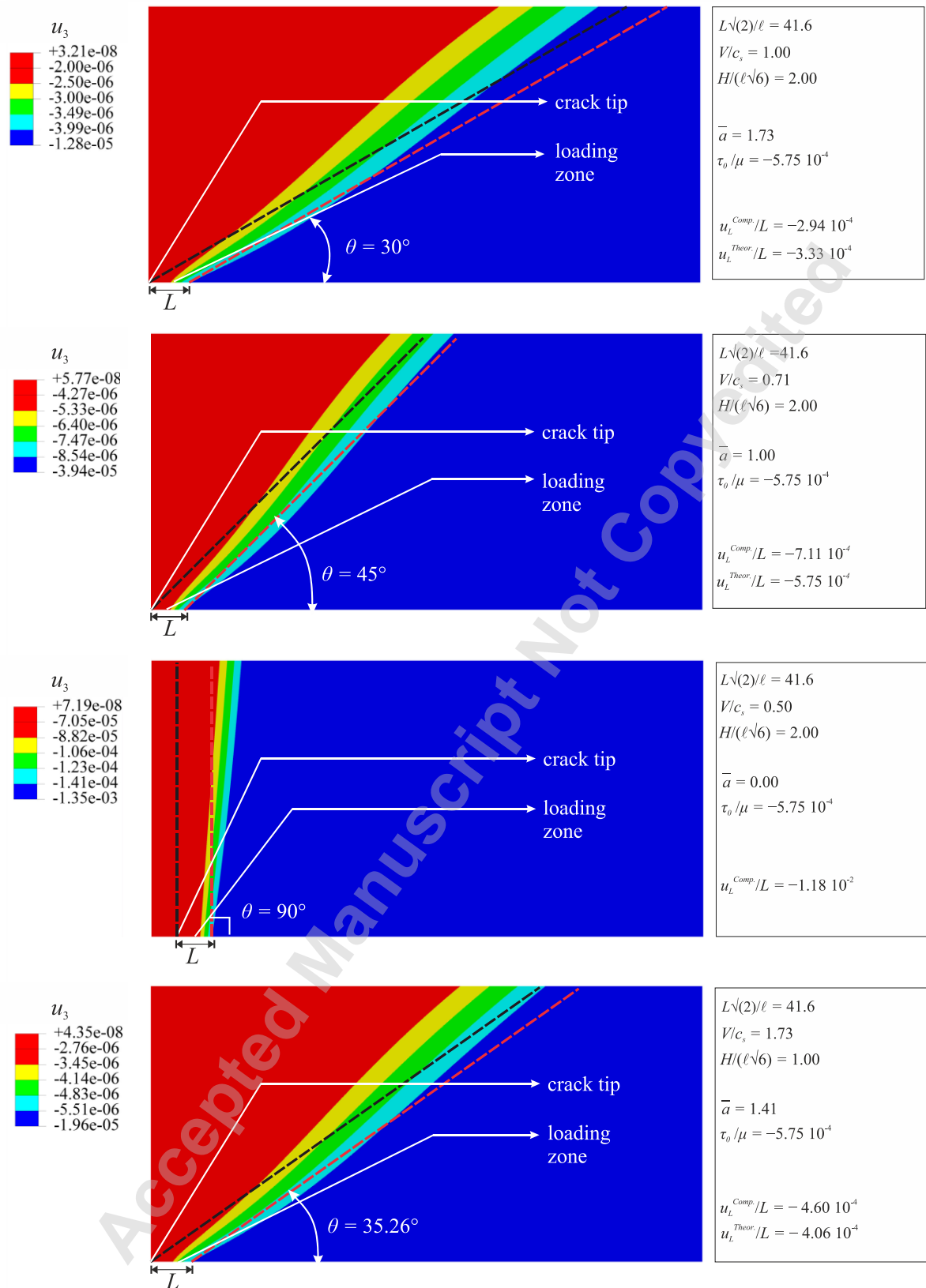
15

Figure 6. The out-of-plane displacement field as computed by FEM. Note the formulation of Mach Cones of slope less than the classic.

16

6. The out-of-plane polarization

In order to calculate the out-of-plane polarization, we note that eq. (3.7) is an inhomogeneous modified Helmholtz equation. The particular solution comes from the out-of-plane displacement $u_3(\bar{\eta})$ which is of the form (4.3.a). This indicates a partial solution for $P_3^{prt}(\bar{\eta})$, which obeys the relation:

$$P_3^{prt} - A\frac{\partial^2 P_3^{prt}}{\partial \bar{\eta}^2} = B\frac{\partial^2 u_3}{\partial \bar{\eta}^2} \tag{6.1.a}$$

$$A = \frac{V^2 H^2}{12\ell^2 c_s^2} > 0.5 \tag{6.1.b}$$

$$B = \frac{V^2}{\ell^2}\frac{\rho(e_{44}-f_{12})}{a\mu} = \frac{V^2}{c_s^2}\frac{(e_{44}-f_{12})}{a\ell^2} \tag{6.1.c}$$

The complete solution of the polarization field can be constructed as superposition of the partial solution (prt) and a homogeneous solution (hmg) that modifies the solution in order to agree with the boundary condition [79]

$$P_3(\xi,\eta) = P_3^{prt}(\bar{\eta}) + P_3^{hmg}(\xi,\eta) \tag{6.2}$$

The original boundary value problem (3.3) could satisfy the boundary condition;

$$P_3(\xi,\eta=0) = \begin{cases} \langle\xi\rangle^0 P_{\max}, & -\infty < \xi < \infty, \quad \eta \geq 0 \\ -\langle\xi\rangle^0 P_{\max}, & -\infty < \xi < \infty, \quad \eta < 0 \end{cases} \tag{6.3}$$

where $\langle ... \rangle^0$ is the Macauley brackets of zeroth order. This boundary condition (B.C.) implies that as the crack propagates, polarized material of limiting polarization P_{max} remains on the crack surfaces [80]. Recently, Wang et al. [81] have observed huge polarization around stationary crack tips in $SrTiO_3$, using scanning transmission electron microscopy. In fact, they observed an average polarization of $62\,\mu C/cm^2$ in three atomic unit cells adjacent to the crack-tip. However, environment may change $P_{\max}$ to a lower value.

The normalized partial solution for polarization can be found by solving eq. (6.1.a) with the condition $P_3^{prt} = 0$ and $\partial P_3^{prt}/\partial\bar{\eta} = 0$ for $\xi \leq 0$ (ahead of the crack-tip);

$$\frac{P_3^{prt}(\bar{\eta})}{u_L B/2} = \frac{\left(-e^{+\frac{\bar{\eta}}{\sqrt{A}}} + e^{-\frac{\bar{\eta}}{\sqrt{A}}}\right)\left\langle\frac{\bar{\eta}}{\sqrt{A}}-0\right\rangle^0 + \left(e^{+\frac{\bar{\eta}-L/\ell}{\sqrt{A}}} - e^{-\frac{\bar{\eta}-L/\ell}{\sqrt{A}}}\right)\left\langle\frac{\bar{\eta}}{\sqrt{A}}-\frac{L/\ell}{\sqrt{A}}\right\rangle^0}{\left(L/\ell\right)} \tag{6.4}$$
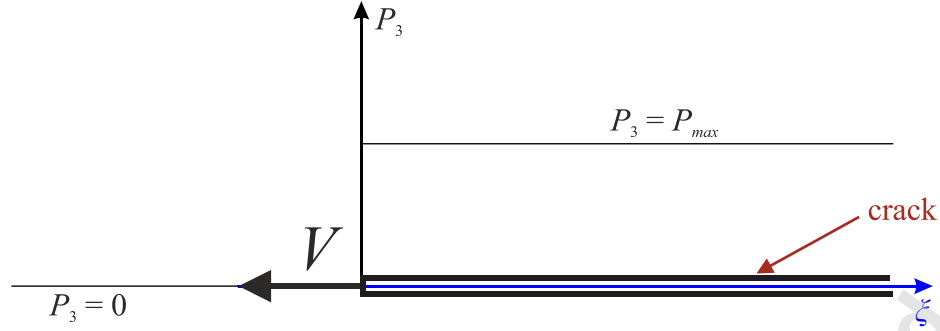
Figure 7. The boundary condition associated with the out-of-plane polarization. The crack-tip is moving in the negative ξ with rapture velocity V. This boundary condition implies that as the crack propagates, it leaves on the crack surfaces polarized material of limiting polarization P_{max} [80].

Accordingly, the homogeneous boundary value problem takes the form;

$$P_3^{hmg} - \frac{\ell^2}{2}\left(\frac{\partial^2 P_3^{hmg}}{\partial \xi^2} + \frac{\partial^2 P_3^{hmg}}{\partial \eta^2}\right) = 0 \tag{6.5}$$

with the following B.C.:

$$P_3^{hmg}(\xi, \eta = 0) = \langle \xi \rangle^0 P_{max} - P_3^{prt}(\bar{\eta} = \xi) = g(\xi), \quad -\infty < \xi < \infty \tag{6.6}$$

The solution of the homogeneous boundary value problem can be represented using the Fokas method as [82–84]:

$$P_3^{hmg}(\xi, \eta) = 2\int_{-\infty}^{\infty} \frac{\partial G}{\partial \eta}(\xi - t, \eta) g(t)\, dt \tag{6.7}$$

$$\frac{\partial G}{\partial \eta}(\xi - t, \eta) = \frac{1}{2\pi}\left(\frac{\ell}{\sqrt{2}}\right)^{-1} \frac{\eta}{\sqrt{(\xi - t)^2 + \eta^2}}\, K_1\left(\left(\frac{\ell}{\sqrt{2}}\right)^{-1}\sqrt{(\xi - t)^2 + \eta^2}\right) \tag{6.8}$$

where $K_1(\cdot)$ is the first-order modified Bessel function of second kind. An asymptotic limit can be explicitly found for $s = (\sqrt{2}/\ell)\sqrt{(\xi - t)^2 + \eta^2} \to \infty$, $K_1(s) \simeq \sqrt{\pi/(2s)}\, e^{-s}$ which gives $P_3^{hmg}(\xi, \eta) \to 0$, as expected.

The solution for some selected parameter combinations is shown in Figure 8. Note that the polarization amplitude concentrates close to the Mach lines. The extreme values of P_3 (maximum and minimum) appear also on the Mach lines and are given due to the partial solution:

18

$$P_3^{prt}\left(\overline{\eta}=0\right)=+\frac{Bu_L}{2}\frac{1-e^{-\frac{L/\ell}{\sqrt{A}}}}{\left(L/\ell\right)} \tag{6.9.a}$$

$$P_3^{prt}\left(\overline{\eta}=\frac{L}{\ell}\right)=-\frac{Bu_L}{2}\frac{1-e^{-\frac{L/\ell}{\sqrt{A}}}}{\left(L/\ell\right)} \tag{6.9.b}$$

Then, we can normalize those quantities, as follows:

$$\frac{P_3^{prt}\left(\overline{\eta}=0,\,L/\ell\right)}{6\left(e_{44}-f_{12}\right)/a}\left(\frac{H^2}{L}\right)\left(\frac{\tau_0}{\mu}\right)^{-1}=\pm\frac{A}{\sqrt{2A-1}}\frac{1-e^{-\frac{L/\ell}{\sqrt{A}}}}{\left(L/\ell\right)} \tag{6.10}$$

19

(a) SrTiO$_3$

$u_L /(\ell/\sqrt{2}) = -2.12 \; 10^5$
$P_{max} /(u_L B/2) = 2.98 \; 10^{-7}$

$V/c_s = 1.15$
$H^2/6\ell^2 = 1.69$

$\overline{a} = 1.12$
$L/(\ell/\sqrt{2}) = 4.24$

(b) SrTiO$_3$

$u_L /(\ell/\sqrt{2}) = -2.12 \; 10^5$
$P_{max} /(u_L B/2) = 1.68 \; 10^{-7}$

$V/c_s = 1.54$
$H^2/6\ell^2 = 1.69$

$\overline{a} = 1.73$
$L/(\ell/\sqrt{2}) = 4.24$

(c) SrTiO$_3$

$u_L /(\ell/\sqrt{2}) = -4.24 \; 10^{-1}$
$P_{max} /(u_L B/2) = 1.49 \; 10^{-1}$

$V/c_s = 1.15$
$H^2/6\ell^2 = 1.69$

$\overline{a} = 1.12$
$L/(\ell/\sqrt{2}) = 4.24$

(d) SrTiO$_3$

$u_L /(\ell/\sqrt{2}) = -2.12 \; 10^5$
$P_{max} /(u_L B/2) = 2.98 \; 10^{-7}$

$V/c_s = 1.15$
$H^2/6\ell^2 = 1.69$

$\overline{a} = 1.12$
$L/(\ell/\sqrt{2}) = 7.07$

(e) KTaO$_3$

$u_L /(\ell/\sqrt{2}) = -3.01 \; 10^5$
$P_{max} /(u_L B/2) = -6.18 \; 10^{-8}$

$V/c_s = 0.71$
$H^2/6\ell^2 = 4.45$
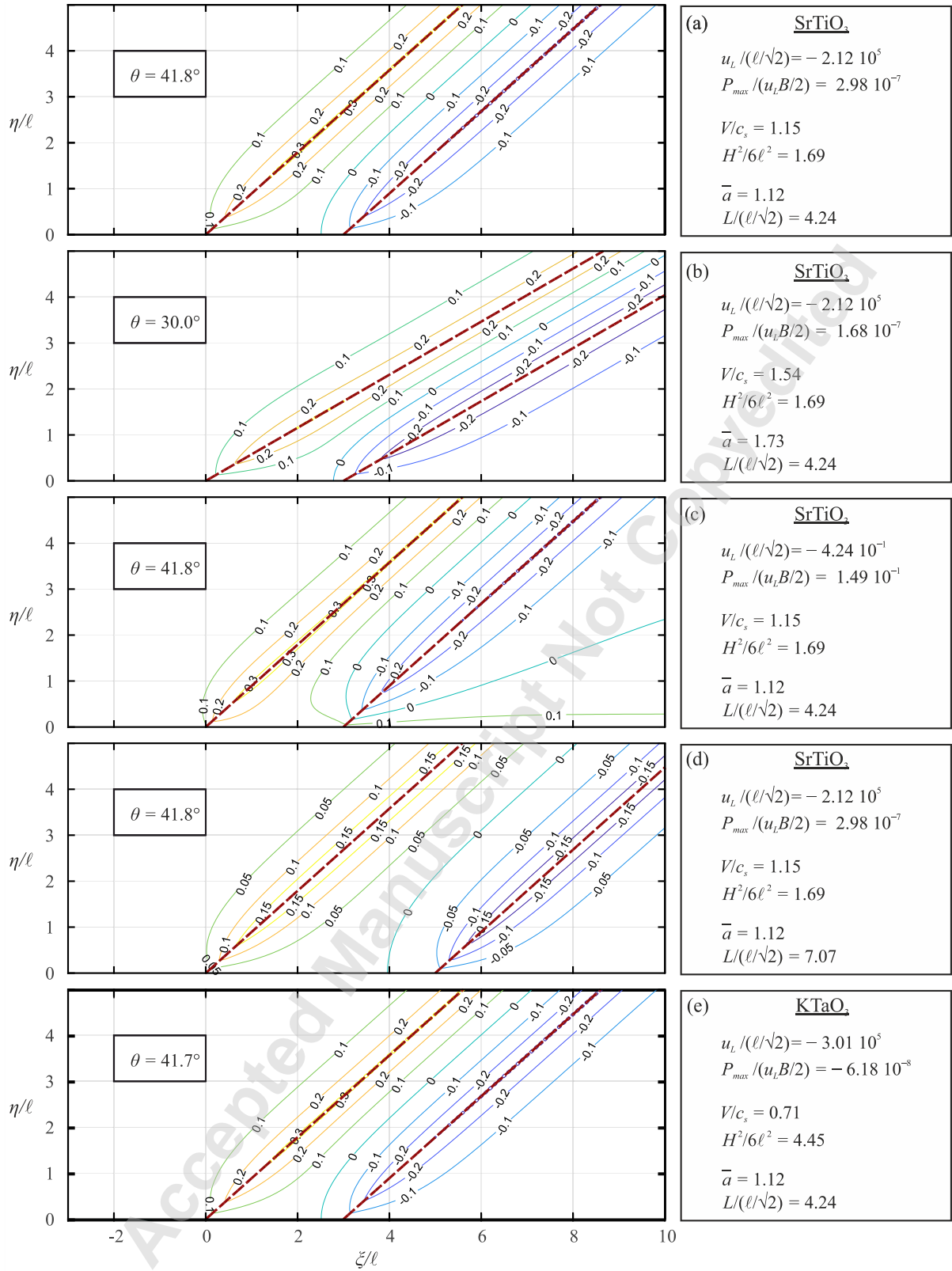
$\overline{a} = 1.12$
$L/(\ell/\sqrt{2}) = 4.24$

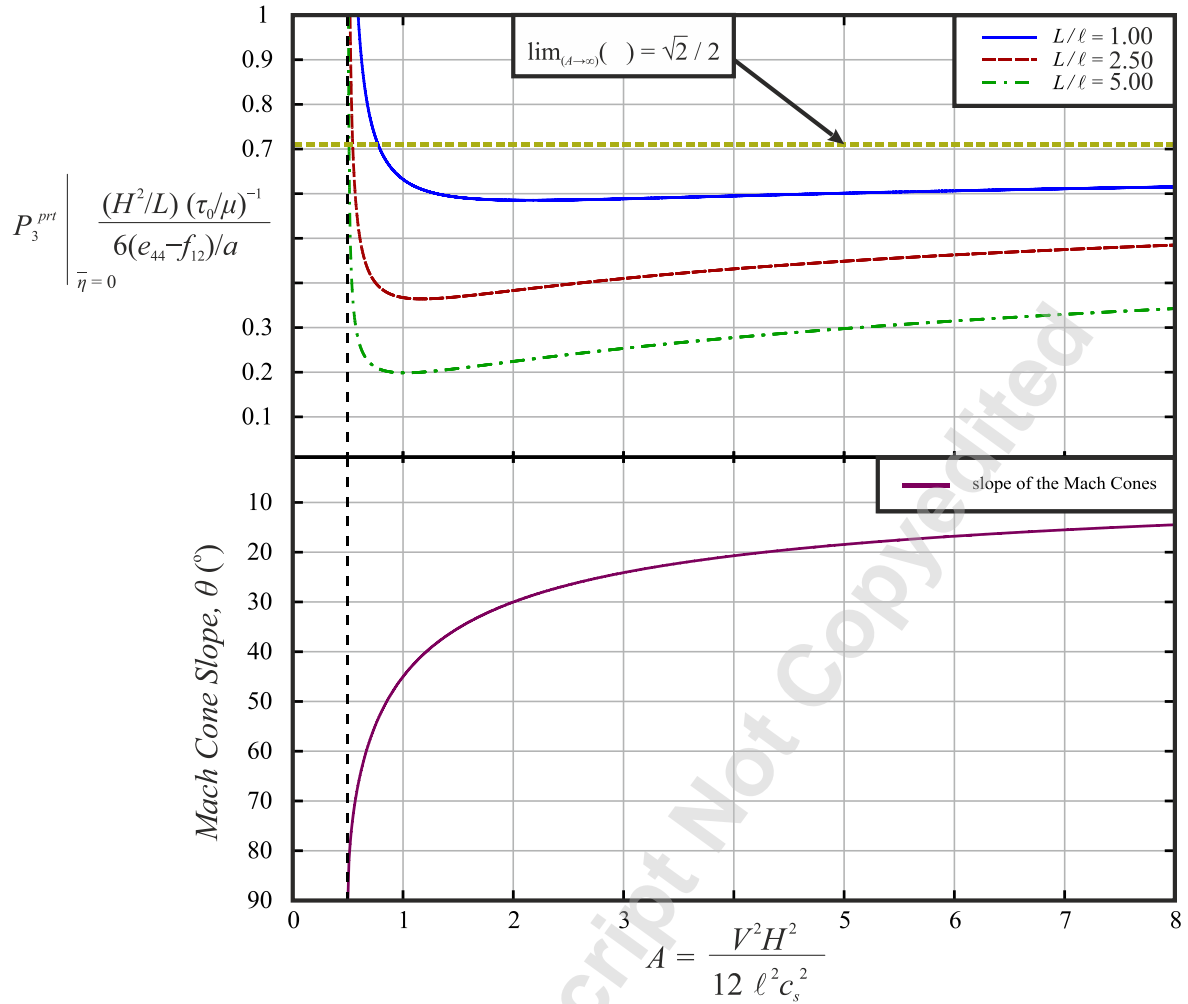Figure 8. The normalized polarization $P_3/(u_L B/2)$ for different rapture velocities V/c_s ($P_{max} > 0$).

Figure 9.   The maximum polarization in respect to the constant A (different velocities), for selected values of the normalized loading region L/ℓ (for $B < 0$ we must take the P_3^{prt} value at $\bar{\eta} = L/\ell$).

The normalized maximum polarization depends strongly on the parameter A (see eqs. (6.1) and (6.9)) and is shown in Figure 9. For $B > 0$ we also show the effect of the parameter A in the Mach cone slope $\theta = \sin^{-1}(VH/(c_s\ell\sqrt{6}))$.

21

7. The Steady State Electromagnetic Response

The steady state magnetic response, i.e. the in-plane magnetic flux $B_\xi(\xi,\eta)$ and $B_\eta(\xi,\eta)$, can be calculated from the polarization $P_3(\xi,\eta)$, as suggested in [41], and particularized by [57]. The equations to be solved for the case of the steady state rapture take the form:

1. Faraday's Law

$$E_{3,\eta} - V\, B_{\xi,\xi} = 0 \tag{7.1.a}$$

$$-E_{3,\xi} - V\, B_{\eta,\xi} = 0 \tag{7.1.b}$$

2. Ampere's Law

$$B_{\eta,\xi} - B_{\xi,\eta} = -V\mu_0\varepsilon_0 E_{3,\xi} - V\mu_0 P_{3,\xi} = 0 \tag{7.2}$$

3. Gauss' Law

$$B_{\xi,\xi} + B_{\eta,\eta} = 0 \tag{7.3}$$

$E_3(\xi,\eta)$ is the steady state out of plane electric field $[\mathrm{A\,m^{-1}\,s^{-1}}]$ and $H_\xi(\xi,\eta)$, $H_\eta(\xi,\eta)$ are the steady state magnetic fields $[\mathrm{A\,m^{-2}}]$. For elastic dielectrics $H_\xi(\xi,\eta) = B_\xi(\xi,\eta)/\mu_0$ and $H_\xi(\xi,\eta) = B_\xi(\xi,\eta)/\mu_0$, where $\mu_0 = 4\pi\,10^{-7}[\mathrm{kg\,m\,C^{-2}}]$ is the magnetic permeability of the vacuum and $\varepsilon_0 = (36\pi)^{-1}\,10^{-9}\ \mathrm{C^2 N^{-1} m^{-2}}$ is the dielectric constant of the vacuum.

Assuming $V^2 c_{light}^{-2} = V^2 \mu_0\varepsilon_0 \ll 1$, we can utilize eq. (7.1.a), (7.1.b), (7.2) and (7.3) to obtain the approximate governing equations of the electromagnetic problem

$$B_{\xi,\xi\xi}\left(1 - V^2\varepsilon_0\mu_0\right) + B_{\xi,\eta\eta} = V\mu_0 P_{3,\xi\eta} \;\;\Rightarrow\;\; \nabla^2 B_\xi \approx +V\mu_0 P_{3,\xi\eta} \tag{7.4.a}$$

$$B_{\eta,\xi\xi}\left(1 - V^2\varepsilon_0\mu_0\right) + B_{\eta,\eta\eta} = -V\mu_0 P_{3,\xi\xi} \;\;\Rightarrow\;\; \nabla^2 B_\eta \approx -V\mu_0 P_{3,\xi\xi} \tag{7.4.b}$$

Equations (7.4.a) and (7.4.b) are of Poisson type with P_3 being now a known function. The solution of (7.4.a) and (7.4.b) in the absence of far field boundary conditions is given as:

$$H_\xi(\xi,\eta) = \frac{V}{4\pi}\int_{-\infty}^{\infty}\int_{-\infty}^{\infty} P_{3,\xi\eta}(\xi',\eta')\ln\left[(\xi-\xi')^2 + (\eta-\eta')^2\right]d\xi'd\eta' \tag{7.5.a}$$

$$H_\eta(\xi,\eta) = -\frac{V}{4\pi}\int_{-\infty}^{\infty}\int_{-\infty}^{\infty} P_{3,\xi\xi}(\xi',\eta')\ln\left[(\xi-\xi')^2 + (\eta-\eta')^2\right]d\xi'd\eta' \tag{7.5.b}$$

The electrical field E_3 can be found using the known magnetic flux $(B_\eta = \mu_0 H_\eta)$, assuming that there is no initial electric field ($B_\eta = 0$, *iff* $E_3 = 0$):

$$E_3 = -V B_\eta \qquad (7.6)$$

H_ξ and H_η (as well as B_ξ and B_η) obtain their maximum values along the leading Mach line and are of the order of $V\mu_0 P_3^{prt}(\overline{\eta} = 0)$. Note, that P_3 also obtains its maximum values along the leading Mach line (see Figure 9). On the other hand, the minimum values of H_ξ and H_η are obtained along the secondary Mach line and are of the order of $V\mu_0 P_3^{prt}(\overline{\eta} = L/\ell)$.
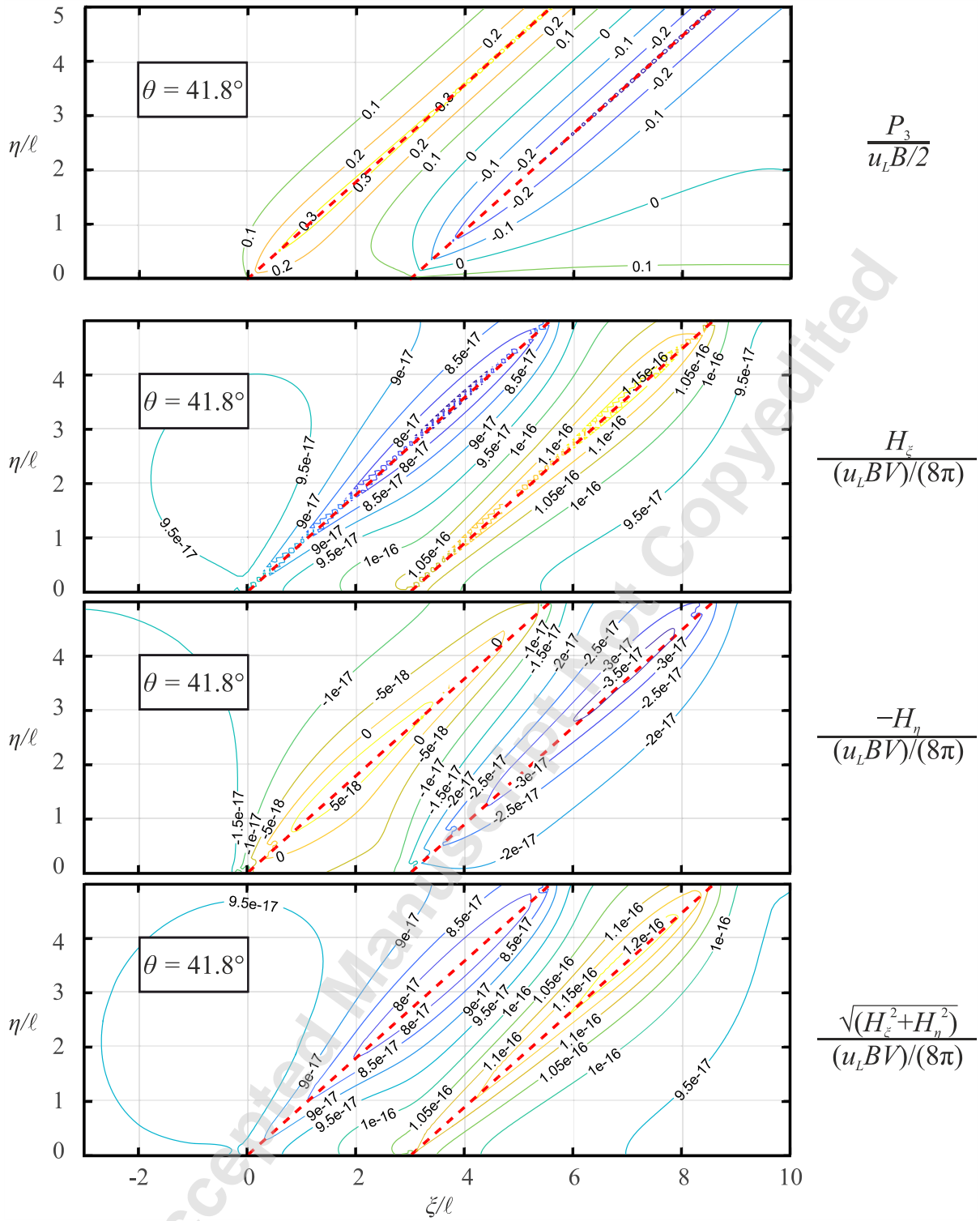
23

Figure 10. The normalized electromagnetic field $H_\xi (8\pi)/(u_L BV)$ and $H_\eta (-8\pi)/(u_L BV)$, and the magnitude of the normalized electromagnetic field $\sqrt{H_\xi^2 + H_\eta^2}/[(8\pi)/(u_L BV)]$ for the material SrTiO$_3$, and also: $u_L/(\ell/\sqrt{2}) = -4.24 \ \ 10^{-1}$, $P_{max}/(u_L B/2) = 1.49 \ \ 10^{-1}$, $V/c_s = 1.15$, $\overline{H}^2/(6\ell^2) = 1.69$, $\overline{a} = 1.12$, $L/(\ell/\sqrt{2}) = 4.24$
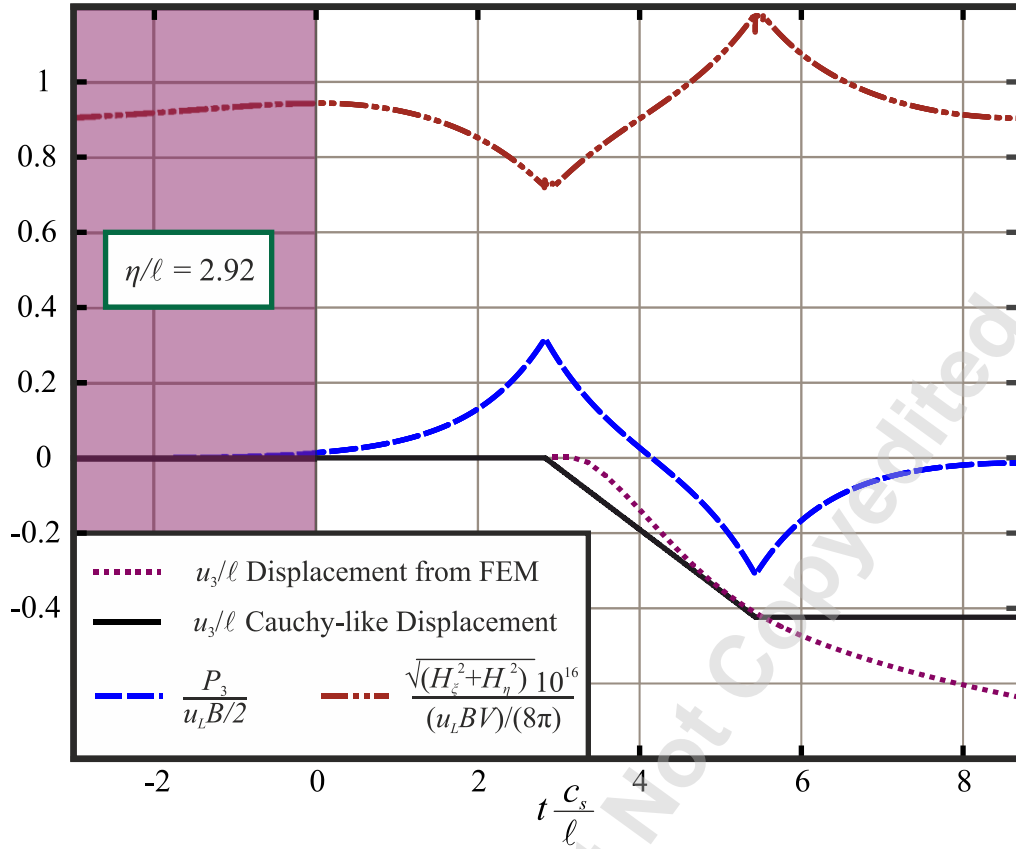
Figure 11. The time history of the Cauchy-like displacement, the polarization and the magnitude of the magnetic field for an observer located in a distance of $\eta = 2.92\ell$ from the crack surface for the case described in Figure 10. Note that the electromagnetic response proceeds the displacement as the observer gets further from the crack surface.

8. Conclusion

The first part of this work examines the mode III hyperbolic steady state rupture regime in magneto-flexoelectric materials. It is shown that hyperbolicity does not necessarily imply the attainment of super-shear rupture speeds in such materials where strain gradients and local length scales are important. It is further shown that unlike classical elastodynamics in the absence process zones super-shear rupture is possible. As a consequence, radiation patterns featuring Mach lines appear at sub-shear as well as super-shear crack ruptures velocities. These Mach lines have been observed in lattice-type atomistic analyses and indicate the important effect of wave dispersion that is present in magneto-flexoelectrics. The analysis can be achieved hierarchically starting with the solution of the mechanical displacement field u_3 which can be subsequently used to obtain the polarization field P_3. Moreover, the polarization field can be used to estimate the accompanying magnetic fields H_ξ, H_η and then to estimate

the electric field E_3. The Mach lines carry the stress, strain and velocity jumps, as well as, the polarization and the magnetic concentrations. The governing hyperbolic partial differential equations were separated into two partial differential equations resembling plate equations and were conveniently modeled as two connected prestressed plates. Accordingly, the problem was numerically solved with the use of a commercial finite element code. The computed radiation patterns and Mach lines were found to agree with the theoretical predictions. The analysis also quantified the electro-magnetic field that accompanies the acoustic shocking.

Acknowledgements

Appendix
A. Shock Wave Analysis

Assume that the motion of a body described in section 3 contains a surface discontinuity, moving with an intrinsic velocity $\overline{U} > 0$ in the normal $\vec{n}$ to the surface direction. The linearity of the problem implies in our case a straight line in the plane (ξ, η). Denote the jump (discontinuity) of a quantity f across this surface as $\|f\| = f^- - f^+$ where f^+, f^- are the values of f immediately in front and immediately behind the surface. We assume in our case that $\|u_3\| = 0$, $\|P_3\| = 0$. From the kinematical condition of compatibility across the jump, we obtain (where $(\cdot)_{,n} = \partial(\cdot)/\partial n$ is the directional derivative):

$$\|\dot{u}_3\| = -\overline{U}\|u_{3,n}\| \quad \text{and} \quad \|\dot{P}_3\| = -\overline{U}\|P_{3,n}\| \tag{A.1}$$

From the traction condition

$$t_3 = \mu\, u_{3,n} + \left(e_{44} - f_{12}\right)P_{3,n} \tag{A.2}$$

we obtain with (A.1) that:

$$\|t_3\| = \left(\mu - \frac{(e_{44} - f_{12})^2}{b_{44} + b_{77}} \right) \|u_{3,n}\| \tag{A.3}$$

Assuming that the intrinsic velocity of the shock is given as in the classic case from the momentum balance (see for example [85]) then:

$$\|t_3\| = -\rho \overline{U} \|\dot{u}_3\| \tag{A.4}$$

Combining eq. (A.4) with eq. (A.3), we have

$$\rho \overline{U}^2 = \mu - \frac{(e_{44} - f_{12})^2}{b_{44} + b_{77}} \tag{A.5}$$

It is trivial to show (using eq. (3.4)) that;

$$\overline{U} = c_s \frac{\ell \sqrt{6}}{H} \tag{A.6}$$

which implies by the shock front slope $\sin \theta = (\ell \sqrt{6} / H)(c_s / V)$, that:

$$\sin \theta = \frac{\overline{U}}{V} \tag{A.7}$$

Then the velocity behind the shock front is related to the traction behind the shock front as:

$$\dot{u}_3 = \frac{t_3}{\rho \overline{U}} \tag{A.8}$$

The kinetic energy density behind the shock front is $(1/2)\rho \dot{u}_3^2$. Utilizing (A.8) and (A.3) we obtain;

$$\frac{1}{2}\rho \dot{u}_3^2 = \frac{1}{2} \frac{t_3^2}{\left(\mu - \frac{(e_{44} - f_{12})^2}{b_{44} + b_{77}} \right)} = \frac{1}{2} t_3 u_{3,n} \tag{A.9}$$

where $u_{3,n}$ is the normal strain deformation behind the shock front. This last expression is the strain energy density. Therefore, on the crack face, the strain energy is transferred directly to the kinetic energy.

B. Couple Stress Boundary Conditions

At $\eta = 0$ and $\xi \geq 0$ couple stress boundary conditions must be applied of the form $\mu_{21} = \mu \ell^2 \, \partial^2 u_3 / \partial \eta^2$ and $-\mu_{22} = (\mu \ell^2 \, \partial^2 u_3) / (\partial \xi \, \partial \eta)$. The plate analogue model implies the in-plane bending moments as in Figure B.1. (at $\xi = 0$ and $\xi = L$) due to the strain and velocity jumps that are allowed along the crack face as indicated in Figure 3. Those moments are:

$$M_{\xi} = 2 \, \bar{a}^2 \mu \, \ell^2 \, \frac{u_L}{L} \tag{B.1}$$

$$M_{\eta} = 2 \, \bar{a} \, \mu \, \ell^2 \, \frac{u_L}{L} \tag{B.2}$$
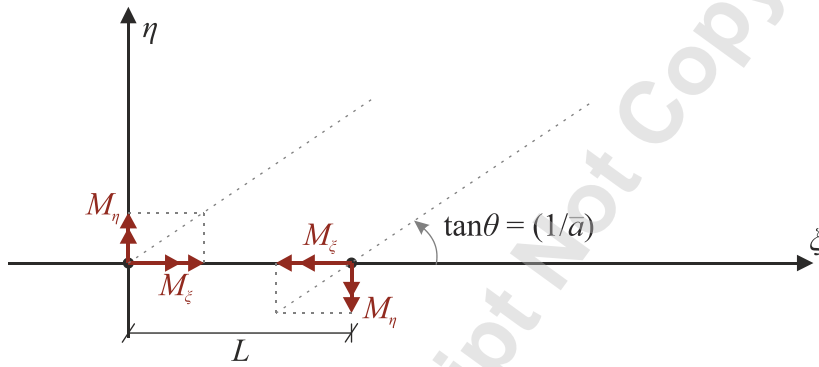

Figure B.1.   The Couple Stress boundary conditions in the form of concentrated moments used for the plate analogue.

References

[1]   Deng, Q., Lv, S., Li, Z., Tan, K., Liang, X., and Shen, S., 2020, "The Impact of Flexoelectricity on Materials, Devices, and Physics," J Appl Phys, **128**(8), p. 080902.

[2]   Wang, B., Gu, Y., Zhang, S., and Chen, L., 2019, "Flexoelectricity in Solids: Progress, Challenges, and Perspectives," Prog Mater Sci, **106**, p. 100570.

[3]   Krichen, S., and Sharma, P., 2016, "Flexoelectricity: A Perspective on an Unusual Electromechanical Coupling," J Appl Mech, **83**(3).

[4]   Yudin, P. v., and Tagantsev, A. K., 2013, "Fundamentals of Flexoelectricity in Solids," Nanotechnology, **24**(43), p. 432001.

[5]   Zubko, P., Catalan, G., and Tagantsev, A. K., 2013, "Flexoelectric Effect in Solids,"
        Annu Rev Mater Res, **43**(1), pp. 387–421.

[6]   Tagantsev, A. K., 1991, "Electric Polarization in Crystals and Its Response to Thermal
        and Elastic Perturbations," Phase Transitions, **35**(3–4), pp. 119–203.

[7]   Majdoub, M. S., Sharma, P., and Cagin, T., 2008, "Enhanced Size-Dependent
        Piezoelectricity and Elasticity in Nanostructures Due to the Flexoelectric Effect," Phys
        Rev B, **77**(12), p. 125424.

[8]   Hu, S., and Shen, S., 2009, "Electric Field Gradient Theory with Surface Effect for
        Nano-Dielectrics," Computers, Materials and Continua, **13**(1), pp. 63–88.

[9]   Shen, S., and Hu, S., 2010, "A Theory of Flexoelectricity with Surface Effect for Elastic
        Dielectrics," J Mech Phys Solids, **58**(5), pp. 665–677.

[10]   Hu, T., Yang, W., Liang, X., and Shen, S., 2018, "Wave Propagation in Flexoelectric
        Microstructured Solids," J Elast, **130**(2), pp. 197–210.

[11]   Tvergaard, V., and Hutchinson, J., 2008, "Mode III Effects on Interface Delamination,"
        J Mech Phys Solids, **56**(1), pp. 215–229.

[12]   Yu, H., and Yang, W., 1994, "Mechanics of Transonic Debonding of a Bimaterial
        Interface: The Anti-Plane Shear Case," J Mech Phys Solids, **42**(11), pp. 1789–1802.

[13]   Gao, H., Huang, Y., Gumbsch, P., and Rosakis, A. J., 1999, "On Radiation-Free
        Transonic Motion of Cracks and Dislocations," J Mech Phys Solids, **47**(9), pp. 1941–
        1961.

[14]   Broberg, K. B., 1989, "The Near-Tip Field at High Crack Velocities," Int J Fract, **39**(1–
        3), pp. 1–13.

[15]   Huang, Y., Liu, C., and Rosakis, A. J., 1996, "Transonic Crack Growth along a
        Bimaterial Interface: An Investigation of the Asymptotic Structure of near-Tip Fields,"
        Int J Solids Struct, **33**(18), pp. 2625–2645.

[16]   Chen, S., and Gao, H., 2010, "Dynamic Behaviors of Mode III Interfacial Crack under
        a Constant Loading Rate," Continuum Mechanics and Thermodynamics, **22**(6–8), pp.
        515–530.

[17]   Burridge, R., 1973, "Admissible Speeds for Plane-Strain Self-Similar Shear Cracks with
        Friction but Lacking Cohesion," Geophys J Int, **35**(4), pp. 439–455.

[18]   Freund, L. B., 1979, "The Mechanics of Dynamic Shear Crack Propagation," J Geophys
        Res, **84**(B5), p. 2199.

[19]   Andrews, D. J., 1976, "Rupture Propagation with Finite Stress in Antiplane Strain," J
        Geophys Res, **81**(20), pp. 3575–3582.

29

[20]   Rosakis, A. J., Samudrala, O., and Coker, D., 1999, "Cracks Faster than the Shear Wave Speed," Science (1979), **284**(5418), pp. 1337–1340.

[21]   Xia, K., Rosakis, A. J., and Kanamori, H., 2004, "Laboratory Earthquakes: The Sub-Rayleigh-to-Supershear Rupture Transition," Science (1979), **303**(5665), pp. 1859–1861.

[22]   Rosakis, A. J., Xia, K., Lykotrafitis, G., and Kanamori, H., 2007, "Dynamic Shear Rupture in Frictional Interfaces: Speeds, Directionality, and Modes," *Treatise on Geophysics*, Elsevier, pp. 183–213.

[23]   Rosakis, A. J., 2002, "Intersonic Shear Cracks and Fault Ruptures," Adv Phys, **51**(4), pp. 1189–1257.

[24]   Burridge, R., Conn, G., and Freund, L. B., 1979, "The Stability of a Rapid Mode II Shear Crack with Finite Cohesive Traction," J Geophys Res, **84**(B5), p. 2210.

[25]   Rosakis, Ph., 2001, "Supersonic Dislocation Kinetics from an Augmented Peierls Model," Phys Rev Lett, **86**(1), pp. 95–98.

[26]   Dunham, E. M., 2007, "Conditions Governing the Occurrence of Supershear Ruptures under Slip-Weakening Friction," J Geophys Res, **112**(B7), p. B07302.

[27]   Liu, Y., and Lapusta, N., 2008, "Transition of Mode II Cracks from Sub-Rayleigh to Intersonic Speeds in the Presence of Favorable Heterogeneity," J Mech Phys Solids, **56**(1), pp. 25–50.

[28]   Rezakhani, R., Rubino, V., Molinari, J. F., and Rosakis, A., 2022, "Three-Dimensional Stress State during Dynamic Shear Rupture Propagation along Frictional Interfaces in Elastic Plates," Mechanics of Materials, **164**, p. 104098.

[29]   Willis, J. R., 1972, "The Penny-Shaped Crack on an Interface," Q J Mech Appl Math, **25**(3), pp. 367–385.

[30]   Gao, H., Huang, Y., and Abraham, F. F., 2001, "Continuum and Atomistic Studies of Intersonic Crack Propagation," J Mech Phys Solids, **49**(9), pp. 2113–2132.

[31]   Guozden, T. M., and Jagla, E. A., 2005, "Supersonic Crack Propagation in a Class of Lattice Models of Mode III Brittle Fracture," Phys Rev Lett, **95**(22), p. 224302.

[32]   Guo, G., Yang, W., and Huang, Y., 2003, "Supersonic Crack Growth in a Solid of Upturn Stress–Strain Relation under Anti-Plane Shear," J Mech Phys Solids, **51**(11–12), pp. 1971–1985.

[33]   Koizumi, H., Kirchner, H. O. K., and Suzuki, T., 2007, "Supersonic Crack Motion in a Harmonic Lattice," Philos Mag Lett, **87**(8), pp. 589–593.

[34]   Guozden, T. M., Jagla, E. A., and Marder, M., 2010, "Supersonic Cracks in Lattice Models," Int J Fract, **162**(1–2), pp. 107–125.

[35]   Archuleta, R. J., 1984, "A Faulting Model for the 1979 Imperial Valley Earthquake," J Geophys Res Solid Earth, **89**(B6), pp. 4559–4585.

[36]   Bouchon, M., and Vallée, M., 2003, "Observation of Long Supershear Rupture During the Magnitude 8.1 Kunlunshan Earthquake," Science (1979), **301**(5634), pp. 824–826.

[37]   Bouchon, M., Bouin, M., Karabulut, H., Toksöz, M. N., Dietrich, M., and Rosakis, A. J., 2001, "How Fast Is Rupture during an Earthquake? New Insights from the 1999 Turkey Earthquakes," Geophys Res Lett, **28**(14), pp. 2723–2726.

[38]   Mello, M., Bhat, H. S., Rosakis, A. J., and Kanamori, H., 2014, "Reproducing the Supershear Portion of the 2002 Denali Earthquake Rupture in Laboratory," Earth Planet Sci Lett, **387**, pp. 89–96.

[39]   Zeng, H., Wei, S., and Rosakis, A., 2022, "A Travel-Time Path Calibration Strategy for Back-Projection of Large Earthquakes and Its Application and Validation Through the Segmented Super-Shear Rupture Imaging of the 2002 Mw 7.9 Denali Earthquake," J Geophys Res Solid Earth, **127**(6).

[40]   Fitterman, D. v., 1979, "Theory of Electrokinetic-Magnetic Anomalies in a Faulted Half-Space," J Geophys Res, **84**(B11), p. 6031.

[41]   Giannakopoulos, A. E., and Rosakis, A. J., 2022, "Dynamic Magneto-Flexoelectricity and Seismo-Electromagnetic Phenomena: Connecting Mechanical Response to Electromagnetic Signatures," J Mech Phys Solids, **168**, p. 105058.

[42]   Varotsos, P., and Alexopoulos, K., 1984, "Physical Properties of the Variations of the Electric Field of the Earth Preceding Earthquakes, I," Tectonophysics, **110**(1–2).

[43]   Yoshida, S., Uyeshima, M., and Nakatani, M., 1997, "Electric Potential Changes Associated with Slip Failure of Granite: Preseismic and Coseismic Signals," J Geophys Res Solid Earth, **102**(B7), pp. 14883–14897.

[44]   Yoshida, S., Clint, O. C., and Sammonds, P. R., 1998, "Electric Potential Changes Prior to Shear Fracture in Dry and Saturated Rocks," Geophys Res Lett, **25**(10), pp. 1577–1580.

[45]   Gokhberg, M. B., Morgounov, V. A., Yoshino, T., and Tomizawa, I., 1982, "Experimental Measurement of Electromagnetic Emissions Possibly Related to Earthquakes in Japan," J Geophys Res, **87**(B9), p. 7824.

[46]   Fenoglio, M. A., Johnston, M. J. S., and Byerlee, J. D., 1995, "Magnetic and Electric Fields Associated with Changes in High Pore Pressure in Fault Zones: Application to the Loma Prieta ULF Emissions," J Geophys Res Solid Earth, **100**(B7), pp. 12951–12958.

[47]   Giannakopoulos, A. E., and Zisis, T., 2021, "Uniformly Moving Antiplane Crack in Flexoelectric Materials," European Journal of Mechanics - A/Solids, **85**, p. 104136.

[48] Ogawa, T., Oike, K., and Miura, T., 1985, "Electromagnetic Radiations from Rocks," J Geophys Res, **90**(D4), p. 6245.

[49] Kobayashi, H., Horikawa, K., Ogawa, K., and Watanabe, K., 2014, "Impact Compressive and Bending Behaviour of Rocks Accompanied by Electromagnetic Phenomena," Philosophical Transactions of the Royal Society A: Mathematical, Physical and Engineering Sciences, **372**(2023), p. 20130292.

[50] Cress, G. O., Brady, B. T., and Rowell, G. A., 1987, "Sources of Electromagnetic Radiation from Fracture of Rock Samples in the Laboratory," Geophys Res Lett, **14**(4), pp. 331–334.

[51] Fifolt, D. A., Petrenko, V. F., and Schulson, E. M., 1993, "Preliminary Study of Electromagnetic Emissions from Cracks in Ice," Philosophical Magazine B, **67**(3), pp. 289–299.

[52] Evtushenko, A. A., Maeno, N., Petrenko, V. F., and Ryzhkin, I. A., 1987, "Pseudopiezoelectric Effects in Ice," Le Journal de Physique Colloques, **48**(C1), pp. C1-109-C1-113.

[53] Petrenko, V. F., 1993, "On the Nature of Electrical Polarization of Materials Caused by Cracks. Application to Ice Electromagnetic Emission," Philosophical Magazine B, **67**(3), pp. 301–315.

[54] Mindlin, R. D., 1968, "Polarization Gradient in Elastic Dielectrics," Int J Solids Struct, **4**(6), pp. 637–642.

[55] Maranganti, R., and Sharma, P., 2009, "Atomistic Determination of Flexoelectric Properties of Crystalline Dielectrics," Phys Rev B, **80**(5), p. 054109.

[56] Giannakopoulos, A. E., and Rosakis, A. J., 2020, "Dynamics of Flexoelectric Materials: Subsonic, Intersonic, and Supersonic Ruptures and Mach Cone Formation," J Appl Mech, **87**(6), p. 061004.

[57] Giannakopoulos, A. E., and Zisis, T., 2021, "Steady-State Antiplane Crack Considering the Flexoelectrics Effect: Surface Waves and Flexoelectric Metamaterials," Archive of Applied Mechanics, **91**(2), pp. 713–738.

[58] Giannakopoulos, A. E., and Zisis, T., 2019, "Uniformly Moving Screw Dislocation in Flexoelectric Materials," European Journal of Mechanics - A/Solids, **78**, p. 103843.

[59] Maranganti, R., Sharma, N. D., and Sharma, P., 2006, "Electromechanical Coupling in Nonpiezoelectric Materials Due to Nanoscale Nonlocal Size Effects: Green's Function Solutions and Embedded Inclusions," Phys Rev B, **74**(1), p. 014110.

[60] Mishuris, G., Piccolroaz, A., and Radi, E., 2012, "Steady-State Propagation of a Mode III Crack in Couple Stress Elastic Materials," Int J Eng Sci, **61**, pp. 112–128.

32

[61] Georgiadis, H. G., 2003, "The Mode III Crack Problem in Microstructured Solids Governed by Dipolar Gradient Elasticity: Static and Dynamic Analysis," J Appl Mech, **70**(4), pp. 517–530.

[62] Koizumi, H., Kirchner, H. O. K., and Suzuki, T., 2007, "Lattice Wave Emission from Moving Cracks," Philosophical Magazine, **87**(27), pp. 4093–4107.

[63] McClintock, F., and Sukhatme, S. P., 1960, "Travelling Cracks in Elastic Materials under Longitudinal Shear," J Mech Phys Solids, **8**(3), pp. 187–193.

[64] Tomizawa, I., and Yamada, I., 1995, "Generation Mechanism of Electric Impulses Observed in Explosion Seismic Experiments.," Journal of geomagnetism and geoelectricity, **47**(3), pp. 313–324.

[65] Curran, D. R., Shockey, D. A., and Winkler, S., 1970, "Crack Propagation at Supersonic Velocities," International Journal of Fracture Mechanics, **6**(3), pp. 271–278.

[66] Winkler, S., Shockey, D. A., and Curran, D. R., 1970, "Crack Propagation at Supersonic Velocities, I," International Journal of Fracture Mechanics, **6**(2), pp. 151–158.

[67] Arakawa, M., Maeno, N., and Higa, M., 1995, "Direct Observations of Growing Cracks in Ice," J Geophys Res, **100**(E4), p. 7539.

[68] Aleksandrov, V. M., and Smetanin, B. I., 1990, "Supersonic Cleavage of an Elastic Strip," Journal of Applied Mathematics and Mechanics, **54**(5), pp. 677–682.

[69] Courant, R., and Lax, A., 1955, "Remarks on Cauchy's Problem for Hyperbolic Partial Differential Equations with Constant Coefficients in Several Independent Variables," Commun Pure Appl Math, **8**(4), pp. 497–502.

[70] Dunham, E. M., 2005, "Near-Source Ground Motion from Steady State Dynamic Rupture Pulses," Geophys Res Lett, **32**(3), p. L03302.

[71] Bonet, J., and Gil, A. J., 2021, "Mathematical Models of Supersonic and Intersonic Crack Propagation in Linear Elastodynamics," Int J Fract, **229**(1), pp. 55–75.

[72] Giannakopoulos, A. E., Knisovitis, C., Zisis, T., and Rosakis A.J., 2023, "Hyperbolicity, Mach Lines and Super-Shear Mode III Steady State Fracture in Magneto-Flexoelectric Materials: II. Crack-Tip Asymptotics (Submitted for Publication)."

[73] Gourgiotis, P. A., and Bigoni, D., 2016, "Stress Channelling in Extreme Couple-Stress Materials Part I: Strong Ellipticity, Wave Propagation, Ellipticity, and Discontinuity Relations," J Mech Phys Solids, **88**, pp. 150–168.

[74] Timoshenko, S. P., and Woinosky-Krieger, S., 1964, *Theory of Plates and Shells (2nd Edition)*.

[75] Katsikadelis, J. T., 1994, "The Analog Equation Method – a Powerful BEM-Based Solution Technique for Solving Linear and Nonlinear Engineering Problems," Transaction on Modeling and Simulation , **7**, pp. 167–182.

[76] Gabet, L., 1993, "The Decomposition Method and Linear Partial Differential Equations," Math Comput Model, **17**(6), pp. 11–22.

[77] Friedman, A., 1958, "Interior Estimates for Parabolic Systems of Partial Differential Equations," Indiana University Mathematics Journal, **7**(3), pp. 393–417.

[78] ABAQUS, 2012, *User Manual*, Hibbit, H. D., Karlsson, B. I., Sorensen, E. P.

[79] Chen, C. S., Jiang, X., Chen, W., and Yao, G., 2015, "Fast Solution for Solving the Modified Helmholtz Equation Withthe Method of Fundamental Solutions," Commun Comput Phys, **17**(3), pp. 867–886.

[80] Yamada, I., Masuda, K., and Mizutani, H., 1989, "Electromagnetic and Acoustic Emission Associated with Rock Fracture," Physics of the Earth and Planetary Interiors, **57**(1–2), pp. 157–168.

[81] Wang, H., Jiang, X., Wang, Y., Stark, R. W., van Aken, P. A., Mannhart, J., and Boschker, H., 2020, "Direct Observation of Huge Flexoelectric Polarization around Crack Tips," Nano Lett, **20**(1), pp. 88–94.

[82] Cheng, H., Huang, J., and Leiterman, T. J., 2006, "An Adaptive Fast Solver for the Modified Helmholtz Equation in Two Dimensions," J Comput Phys, **211**(2), pp. 616–637.

[83] Colbrook, M. J., Ayton, L. J., and Fokas, A. S., 2019, "The Unified Transform for Mixed Boundary Condition Problems in Unbounded Domains," Proceedings of the Royal Society A: Mathematical, Physical and Engineering Sciences, **475**(2222), p. 20180605.

[84] Fokas, A. S., 1997, "A Unified Transform Method for Solving Linear and Certain Nonlinear PDEs," Proceedings of the Royal Society of London. Series A: Mathematical, Physical and Engineering Sciences, **453**(1962), pp. 1411–1443.

[85] Ting, T. C. T., and Li, Y., 1983, "Eulerian Formulation of Transport Equations for Three-Dimensional Shock Waves in Simple Elastic Solids," J Elast, **13**(3), pp. 295–310.